Chemical Engineering Journal 143 (2008) 257–264

Contents lists available at ScienceDirect

Chemical Engineering Journal

journal homepage: www.elsevier.com/locate/cej

Humidification dehumidification desalination process: Design and performance evaluation

Mohammad Al-Sahali, Hisham M. Ettouney*

Department of Chemical Engineering, College of Engineering and Petroleum, Kuwait University, Kuwait

ARTICLE INFO

Article history:
Received 27 May 2007
Received in revised form 9 April 2008
Accepted 16 April 2008

Keywords:
Desalination
Humidification–dehumidification
Heat transfer coefficient
Modeling

ABSTRACT

This paper focuses on the design and modeling of the humidification dehumidification desalination (HDH) process. The process is only found on experimental or very small pilot scale. Literature studies are rather limited and it includes a number of experimental investigations, performance evaluation, and measurements of the heat and mass transfer coefficients. This study includes useful and new data on the evaluation of the heat transfer coefficient of the humid air stream in the condenser unit. The analysis develops a correlation for the heat transfer coefficient for the humid air stream as a function of the Reynolds and Prandtl numbers. Also, detailed evaluation of the system performance is presented as a function of the system temperatures and the inlet relative humidity of the air stream. Results are presented for variations in the humidifier height, heat transfer area of the condenser, flow rate of cooling water, performance ratio (defined as kg of product water per 1 kg of heating steam), and flow rates of the air and water streams. Results show the need for further system optimization through experimental measurements and mathematical modeling to determine the design and operating conditions that provides the lowest unit product cost.

1. Introduction

Limited resources of fresh water are always put under stress due to population increase as well as expansion of urban and industrial developments. The problem is further magnified by pollution due to poor treatment of domestic and industrial wastewater. Examples of over pumping of underground water aquifers and subsequent rapid reduction of the water level are quite common. Moreover, underground water resources near the sea are plagued with seawater intrusion and increase in the water salinity. Also, river courses are diverted and blocked by large dams to generate sufficient head required to operate turbines for generation of electricity. In addition, many countries exist in highly arid zones or experience sustained drought periods. In this regard, industrial desalination is always thought as the most viable solution. Many countries in the Gulf area, the Caribbean, and the Mediterranean, have adopted desalination as a sustainable source of fresh water. At present, the desalination industry is almost equally divided between the reverse osmosis (RO) and the multistage flashing (MSF) processes. A much smaller market share of water desalination is generated by the multiple effect evaporation (MEE) process [1].

Many other desalination processes are only found on experimental/pilot scale or just as a concept design. Adoption of any of these processes is rather difficult because of the competition. The conventional desalination processes, which include the MSF, RO, and MEE, have well-established reliability, extensive field experience, and large production capacities. Irrespective of this, it is highly desirable to continue the research and development work to analyze and study new as well as existing configurations. This should lead to process improvement or development of new and more efficient configurations.

The humidification dehumidification desalination (HDH) process is an attractive desalination process because of its simple layout and it can be combined with solar energy. Also, it can be designed to minimize the amount of energy discarded to the surroundings. Goosen et al. [2] reviewed various layouts of the humidification dehumidification desalination systems as well as single and multiple effect solar desalination. The authors stressed the fact that many of these units are limited to theoretical evaluation or prototype scale; however, increase in future demand for fresh water might make several of these processes viable for fresh water production. Muller-Holst et al. [3] described the performance of an optimized humidification–dehumidification desalination sys-

* Corresponding author at: Department of Chemical Engineering, College of Engineering and Petroleum, Kuwait University, P.O. Box 5969, Safat 13060, Kuwait. Tel.: +965 6024661; fax: +965 4839498.
E-mail address: hisham@kuc01.kuniv.edu.kw (H.M. Ettouney).

1385-8947/$ – see front matter © 2008 Elsevier B.V. All rights reserved.
doi:10.1016/j.cej.2008.04.030

Nomenclature

a_h	specific mass transfer area in humidifier (m^2/m^3)
A	area (m^2)
Cp	specific heat at constant pressure (kJ/(kg K))
d	tube diameter (m)
h	heat transfer coefficient (kW/(m^2 °C))
H	air enthalpy (kJ/kg)
k	thermal conductivity (kW/(K m))
K_y	overall mass transfer coefficient of water in air (kg/(s m))
L	length or height (m)
LMTD	logarithmic mean temperature difference (°C)
M	mass flow rate (kg/s)
$\tilde{M}$	molecular weight, (kg/kmol)
Nu_a	Nusslet number for the air stream, $Nu_a = h_a d_o/k_a$ (dimensionless)
p	pressure (kPa)
Pr	Prandtl number, $Pr = \mu Cp/k$ (dimensionless)
Q	thermal load (kW)
r	tube radius (m)
R	universal gas constant (m^3 kPa/(mol K))
Re	Reynolds number, $Re = \rho V d_o/\mu$ (dimensionless)
T	temperature (°C)
U	overall heat transfer coefficient (kW/(m^2 °C))
V	velocity (m/s)
W	absolute humidity of air (kg H_2O/kg dry air)

Greek symbols

λ	latent heat for evaporation (kJ/kg)
μ	dynamic viscosity (kg/(m s))
ρ	density (kg/m^3)
ϕ	relative humidity (dimensionless)

Subscripts

a	air
am	ambient conditions
c	condenser
cw	cooling water
d	distillate product water
db	dry
i	inlet stream
h	humidifier
o	outlet stream
s	heating steam
st	saturation conditions
w	water
wh	preheater

tem. A main feature of this patent configuration is that the flow of the air stream is driven by natural convection. The system is also associated with a solar collector. Therefore, continuous operation of the unit requires the use of a heat storage system. The system is designed for operation in remote areas with minimal maintenance requirements. This is achieved in part by low temperature operation, which minimizes the rate of scale formation. Farid and Al-Hajaj [4] constructed a small-scale humidification dehumidification unit with a capacity of 2 L/m^2. The system utilized a combination of a water heater and a solar collector. Other studies by Al-Hallaj et al. [5] and Nawayseh et al. [6–8] covered additional aspects, which include modeling, evaluation of the heat and mass transfer coefficients, and field performance. Al-Enezi et al. [9] measured the performance of a humidification dehumidification system at low temperatures. They reported a low conversion ratio of less than 0.01 kg product per 1 kg water flowing in the humidifier. They also reported measured the overall heat transfer coefficient in the condenser and the overall mass transfer coefficient in the humidifier. Ettouney [10] analyzed several layouts for the humidification dehumidification process, which includes the conventional system combined with either one of the following units to condense/extract the water vapor from the air: (1) water condenser, (2) membrane air drying, (3) vapor compressor, and (4) lithium bromide absorption desorption. Analysis of these four configurations shows the need for further evaluation and optimization to determine the most efficient design and operating conditions that generate the lowest product cost.

Common findings among various literature studies indicate that the production rate of distillate water is increased upon the increase of the hot water temperature. On the other hand, the production rate of the distillate water exhibit a maximum upon increase of the air and water flow rates. In all cases increasing the air or water flow rates would enhance mixing within the system and increases the humidification rate. At higher water or air flow rates the evaporation efficiency is decreased because of the increase in the sensible heat load of the system. This would reduce the water evaporation rate and humidification efficiency. Reduction of the condenser heat transfer area requires use of finned tube configuration. This is necessary because of the low heat transfer coefficient on the air side; this is irrespective of water vapor condensation, which account for a very small percentage of the entire air stream.

This paper includes development of a heat transfer coefficient correlation for the humidified air on the shell side of the air condenser. The correlation is developed as a function of the Reynolds and Prandtl numbers of the air stream. This is followed by design and performance evaluation of the air humidifier and condenser over a range of operating parameters. The results are presented in terms of variations in the performance ratio, the condenser specific heat transfer area (defined as the ratio of the heat transfer area to distillate production rate), the specific flow rate of the cooling water (defined as the mass flow rate ratio of cooling water and distillate product), and other system parameters.

2. Description of the HDH process

A schematic of the HDH process is shown in Fig. 1. The process includes three main parts. These are the air humidifier, the condenser, and the feed water heater. The air humidifier contains packing material, either plastic rings or structured packing. This is necessary to increase the contact area between the air and water streams. The packing material is placed in more than one bed and

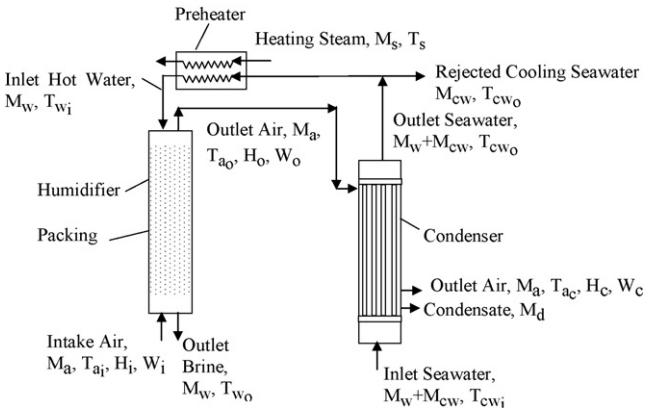

Fig. 1. Conventional humidification dehumidification desalination process.

Table 1
Values of design and operating parameters

Parameter	Symbol	Value	Units
Inner diameter of condenser tubes	d_i	0.025	m
Outer diameter of condenser tubes	d_o	0.03	m
Length of condenser tubes	L_c	1	m
Cross-section area of the humidifier	A_h	4	m^2
Thermal conductivity of condenser tubes	k_w	0.04	kW/(m K)
Flow rate of cold water	M_{cw}	0.003–0.007	kg/s
Flow rate of dry air	M_a	0.0013–0.0034	kg/s
Overall mass transfer coefficient of the water vapor in the air stream	$K_y a_h$	0.354	kg/(s m^2)
Relative humidity of air entering the humidifier	W_{ai}	10–90%	
Relative humidity of air entering the condenser	W_{ao}	100%	
Relative humidity of air leaving the condenser	W_c	100%	
Heating steam temperature	T_s	$T_{wi}+10$	°C
Temperature of hot water entering the humidifier	T_{wi}	60–90	°C
Temperature of hot water leaving the humidifier	T_{wo}	40	°C
Temperature of dry air entering the humidifier	T_{ai}	25–50	°C
Temperature of dry air leaving the humidifier	T_{ao}	T_{wi}–20	°C
Temperature of dry air leaving the condenser	T_c	$T_{cwi}+10$	°C
Inlet temperature of cooling water	T_{cwi}	25	°C
Outlet temperature of cooling water	T_{cwo}	$T_{ao}-5$	°C

the beds are separated by perforated redistribution plates. Typical condenser design for air/water system usually calls for the use of finned tubes on the air side. The cooling water flows on the tube side. This would facilitate the cleaning process to remove scaling or fouling material. For the same reasons, the preheater unit routs the water stream on the tube side and the condensing steam on the shell side.

Condensation of the water vapor from the air stream takes place on the shell side. This results in the increase of the temperature of the seawater stream. Part of the seawater stream leaving the condenser is discarded and the remaining part flows through the preheater. The preheater increases the water temperature to the desired design value before entering the humidifier. The hot water stream is then sprayed at the top of the humidification column in a counter current flow pattern against the intake ambient air stream. The humidified warm air stream then flows on the shell side of the condenser.

The preheater energy can be supplied by solar collectors, process heating steam, diesel engine, other forms of renewable energy, or low grade energy available in industrial sites. The input energy is discarded to the surroundings in the outlet air stream leaving the condenser, the cooling seawater stream leaving the condenser, and the outlet water stream leaving the humidifier. Efficient energy use requires that the temperature difference of these three streams is not more than 5–10 °C higher than that of the intake seawater [11,13]. Therefore, the minimum amount of energy is discarded to the surroundings.

3. Data analysis

The experimental system is operated over a range of temperatures and flow rates of air and water. These parameters together with the condenser and humidifier dimensions are shown in Table 1. Data analysis includes calculations of the condenser thermal load, which is given by

$$Q_c = (M_{cw} + M_w)Cp_{cw}(T_{cw_o} - T_{cw_i}) \quad (1)$$

The condenser thermal load is then used together with the logarithmic mean temperature difference

$$LMTD_c = \frac{(T_{a_o} - T_{cw_o}) - (T_{a_c} - T_{cw_i})}{\ln((T_{a_o} - T_{cw_o})/(T_{a_c} - T_{cw_i}))} \quad (2)$$

to determine the overall heat transfer coefficient between the cooling water and the humidified air stream

$$U_c = \frac{Q_c}{A_c\, LMTD_c} \quad (3)$$

The overall heat transfer coefficient is then used to calculate the heat transfer coefficient on the humidified air side. This is given by the following equation

$$\frac{1}{h_a} = \frac{r_o/r_i}{1/U_c - 1/h_{cw} - (r_i/k_w)\ln(r_o/r_i)} \quad (4)$$

In Eq. (4), the heat transfer coefficient on the water side is obtained from the Dittus–Boelter correlation

$$h_{cw} = 0.023(Re_{cw})^{0.8}(Pr_{cw})^{0.333}\left(\frac{k_{cw}}{d_i}\right) \quad (5)$$

Calculations of the Reynolds and Prandtl numbers for the water stream requires determination of the following water properties as a function of temperature; thermal conductivity, specific heat at constant pressure, density, and dynamic viscosity. Correlations for the water physical properties are given in Appendix A.

The measured values of the heat transfer coefficient on the humid air side are correlated in a dimensionless form as a function of the Reynolds and Prandtl numbers for the air stream. It should be noted that the Reynolds and Prandtl numbers are obtained as a function of the air physical properties, which includes thermal conductivity, specific heat at constant pressure, density, and dynamic viscosity. Correlations for these properties are given in Appendix A. The resulting correlation for the air Nusselt number is given by

$$Nu_a = 1.019 \times 10^{-14}(Re_a)^{0.4806}(Pr_a)^{-95.69} \quad (6)$$

The coefficient of determination (R^2) value for the above correlation is 0.93. The correlation is valid for the design and operating conditions shown in Table 1. Variations in the calculated and measured Nusselt numbers are shown in Fig. 2.

The developed correlation is used to determine variations in the heat transfer coefficient for the humid air as function of various operating parameters. These calculations are made over the parameters range used in the experiments. Fig. 3 shows the effect of the air flow rate and the inlet air temperature on the heat transfer coefficient. As shown, the heat transfer coefficient increases with the increase in the air temperature and the air flow rate. This is because increasing the air temperature reduces the viscosity and increases the thermal conductivity of the air and water streams and in turn reduces the resistance to heat transfer. Variations in

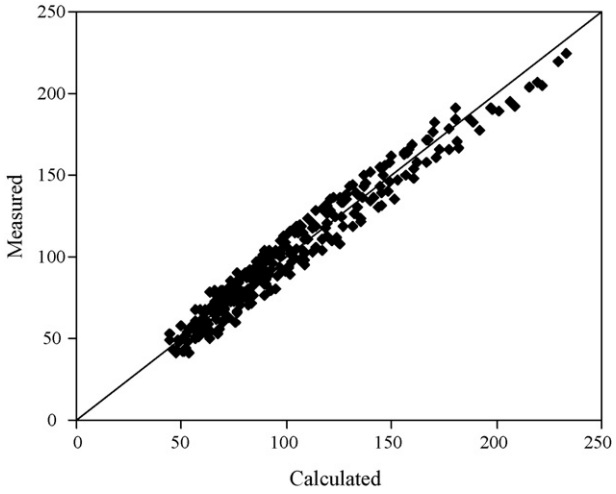

Fig. 2. Variation in measured and calculated air Nusselt number.

the humid air heat transfer coefficient as a function of the air flow rate and cold water temperature are shown in Fig. 4. As shown, a similar behavior to that shown in Fig. 3 is observed, where the heat transfer coefficient of the humid air increases upon the increase of the cold water temperature and the air flow rate. The effect of the air and water flow rates on the heat transfer coefficient is shown in Fig. 5. As shown, increases in both parameters increase the heat transfer coefficient. This is because of the increase in the Reynolds number for both streams, which results in the reduction of the heat transfer resistance.

It should be stressed that the heat transfer coefficient data are obtained for a double pipe configuration. Such arrangement cannot be used in real systems because of the small heat transfer coefficient on the humid air side. Therefore, actual systems would use finned tube condensers. An area ratio of the fins to the tubes would range from 10 to 40 [11]. Irrespective of this, it should be noted that the heat transfer coefficient measured in this study is almost 10 times larger than that for dry air. Therefore, it is necessary to continue the measurements and analysis for the case of humid air with water vapor condensation on finned tubes.

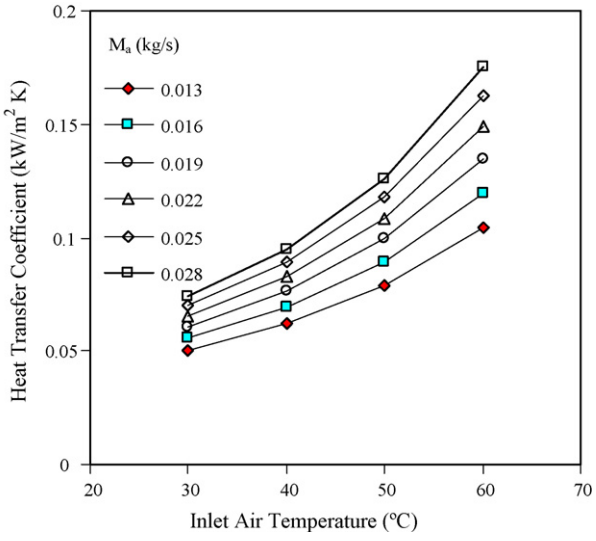

Fig. 3. Variation in the air heat transfer coefficient as a function of the inlet air temperature and air mass flow rate.

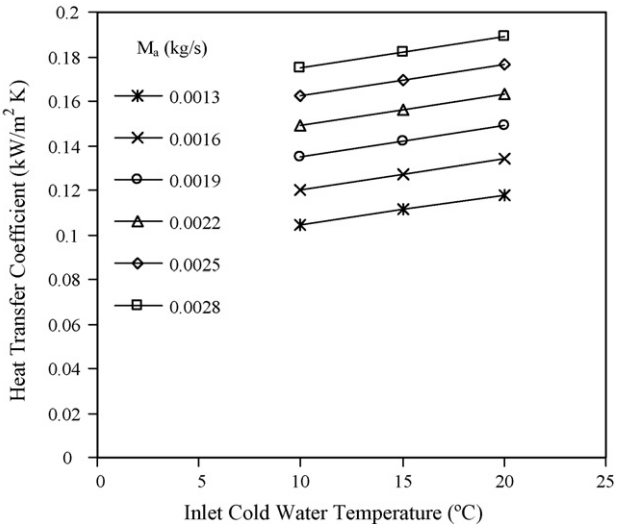

Fig. 4. Variation in the air heat transfer coefficient as a function of the inlet cold water temperature and air mass flow rate.

4. Mathematical model of the HDH process

Analysis of the conventional HDH system includes design of the humidifier, condenser, and preheater. Modeling of these units assumes steady state operation and negligible heat losses to the surroundings. Also, it is assumed that the air stream leaving the humidifier and the condenser are saturated with water vapor. The humidifier height is obtained following the model developed by Foust et al. [12], which is given by

$$L_h = \frac{2M_w Cp_w M_a^2 (C_1 - C_2)}{C_s K_y a_h A_h} \quad (7)$$

The parameters shown in Eq. (7) are defined by the following relations:

$$C_1 = \text{ATAN}\left(\frac{(311.0344\, T_{w_i} + B_1)}{B_s}\right)$$

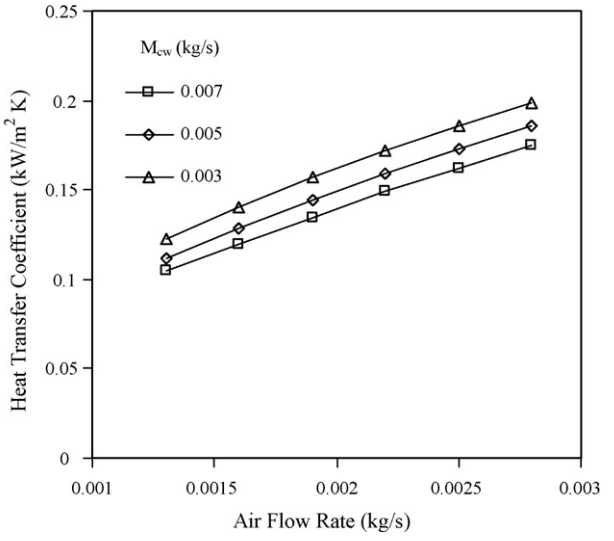

Fig. 5. Variation in the air heat transfer coefficient as a function of the flow rates of the dry air and cold water streams.

$$C_2 = \text{ATAN}\left(\frac{(311.0344\,T_{w_o} + B_1)}{B_s}\right)$$

$$B_s = (622.0688\,B_o - B_1^2)^{1/2}$$

$$B_o = 69344.83 - H_{a_i} + M_w \text{Cp}_w M_a T_{w_o}$$

$$B_1 = -3689.66 - M_w \text{Cp}_w M_a$$

The energy balance equations for the condenser, humidifier, and preheater are given by

$$(M_w + M_{cw})\text{Cp}_{cw}(T_{cw_o} - T_{cw_i}) = M_a(H_o - H_c) \quad (8)$$

$$M_a(H_{a_o} - H_{a_i}) = M_w \text{Cp}_w(T_{w_i} - T_{w_o}) \quad (9)$$

$$M_s\lambda_s = M_w \text{Cp}_w(T_{w_i} - T_{cw_o}) \quad (10)$$

The heat transfer areas of the condenser and heater are given by the following relations:

$$(M_w + M_{cw})\text{Cp}_{cw}(T_{cw_o} - T_{cw_i}) = U_c A_c\ \text{LMTD}_c \quad (11)$$

$$M_s\lambda_s = U_{wh} A_{wh}\ \text{LMTD}_{wh} \quad (12)$$

In Eqs. (11)–(12) the logarithmic mean temperature difference

$$\text{LMTD}_c = \frac{(T_{a_o} - T_{cw_o}) - (T_{a_c} - T_{cw_i})}{\ln((T_{a_o} - T_{cw_o})/(T_{a_c} - T_{cw_i}))} \quad (13)$$

$$\text{LMTD}_{wh} = \frac{(T_{cw_o} - T_{w_i})}{\ln((T_s - T_{w_i})/(T_s - T_{cw_o}))} \quad (14)$$

The fresh water production rate is given by the mass balance in the condenser

$$M_d = M_a(W_c - W_o) \quad (15)$$

The specific flow rate of cooling water and the specific heat transfer area for the entire system are given by the following relations:

$$sM_{cw} = \frac{M_{cw}}{M_d} \quad (16)$$

$$sA = \frac{A_{wh} + A_c}{M_d} \quad (17)$$

Solution of Eqs. (7)–(17) gives the humidifier length and the flow rates of the water flowing in the humidifier, the cooling water in the condenser, heating steam, and the air. Also, it gives the heat transfer areas of the condenser and heater. Solution of Eqs. (7)–(17) requires definition of the air enthalpy, the air absolute humidity, the water latent heat, and the water specific heat. The air enthalpy is expressed in terms of the air temperature and humidity

$$H_a = (\text{Cp}_a + \text{Cp}_v W_a)T_a + \lambda_v W_a \quad (18)$$

The air absolute humidity is given as a function of the atmospheric pressure and vapor pressure at the dry bulb temperature

$$W = 0.62198\frac{p_{db}}{p_{am} - p_{db}} \quad (19)$$

The water vapor pressure at the dry bulb temperature

$$p_{db} = \phi p_{st} \quad (20)$$

The correlations used in the above model, which includes the specific heat at constant pressure for air and water, the water vapor saturation pressure, the latent heat of evaporation/condensation of water vapor are given in Appendix A.

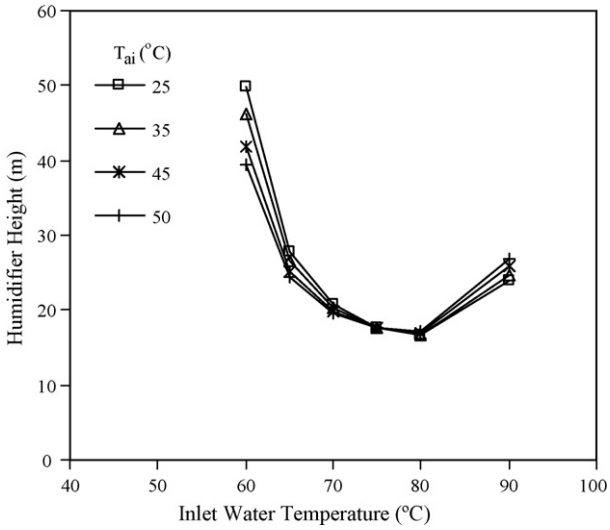

Fig. 6. Variation in the column height as a function of the intake air temperature and inlet water temperature.

5. Results and discussion

System design and performance are analyzed for constant capacity system of 100 m^3/d of product distilled water. The analysis is presented in terms of variations in the humidifier height, the flow rates of air and water, the condenser heat transfer area, the flow rate of the cooling water, and the performance ratio. These calculations are performed for the parameters range shown in Table 1. Figs. 6 and 7 show variations in humidifier height as a function of the inlet relative humidity of the air stream and the inlet temperatures of the air and water streams. The results shown in Fig. 6 are obtained for a constant inlet air humidity of 10%. As shown at low humidity, variations in the humidifier height have negligible dependence on the inlet air temperature. Increase in the inlet air humidity makes the humidifier height more sensitive to variations in the inlet air temperature. These results are shown in Table 2 for an inlet air temperature and relative humidity of 25–50 °C and 10–90%. These results show that the percentage increase in the humidifier

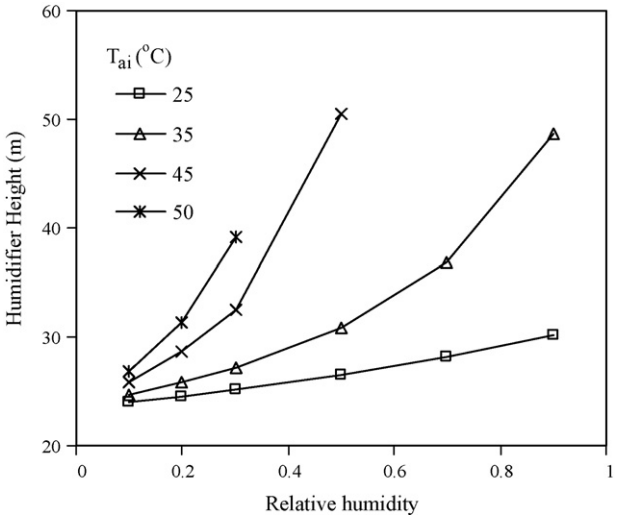

Fig. 7. Variation in the column height as a function of the intake air temperature and relative humidity.

Table 2
Variations in the humidifier height as a function of the inlet air temperature and relative humidity

Inlet air temperature (°C)	Humidifier height (m)			
	10%[a]	30%[a]	50%[a]	90%[a]
25	24.00	25.13	26.47	30.1
30	24.29	25.96	28.12	35.15
35	24.67	27.21	30.92	48.59
40	25.19	29.17	36.32	–
45	25.91	32.50	50.46	–
50	26.91	39.10	361.82	–

[a] Inlet air relative humidity.

height is close to 100% as the inlet air humidity increases from 10% to 90% at an inlet air temperature of 35 °C. For an existing system this would imply reduction in the system productivity by approximately 50%. It should be noted long spells of high relative humidity might be experienced in hot and arid climates; at such conditions the air temperature will not exceed 35 °C. On the other, a temperature range of 40–50 °C, which is common during the summer months in the Gulf countries, are usually associated with relative humidity below 20%.

As shown in Fig. 6, the column height varies considerably as a function of the inlet water temperature. A minimum humidifier height is obtained at an inlet water temperature of 80 °C. This behavior is caused by the larger specific heat of water stream. Variations in the humidifier height as a function of the inlet air temperature and humidity are shown in Fig. 7. As shown, the humidifier height is slightly affected by the inlet air humidity at low inlet air temperatures. In actual practice a humidifier height is constant. Also, the relative humidity of the inlet air stream is an ambient property and can only be altered if an air dryer/humidifier is placed ahead of the humidifier. This might not be a feasible idea, therefore, the design data shown in Figs. 6 and 7, might call for system operation at high/low/medium inlet air humidity. This can be achieved through simultaneous adjustment of the inlet air and water flow rates. This should take into consideration the need for constant production capacity of the fresh water product.

Variations of the air and water flow rates as a function of the inlet temperatures of the air and water stream are shown in Fig. 8. As shown, the flow rates strongly depends on the water temperature and decrease upon increase of the water temperature. Increasing

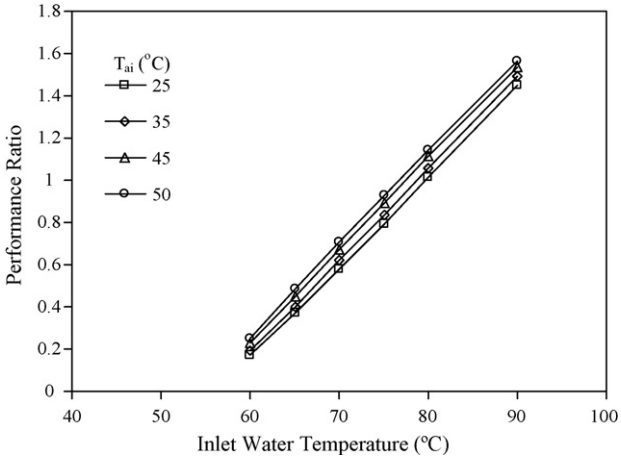

Fig. 9. Variation in the performance ratio as a function of the inlet temperatures of the air and water streams.

the water or the air temperatures would increase the driving force for heat and mass transfer. As a result, a lower flow rate of air and water would be required to generate the same amount of product. A similar behavior is also found for variations of the system performance ratio, see Fig. 9.

Variations in the condenser properties are shown in Figs. 10 and 11. As shown, the specific flow rate of cooling water increases with increase in the inlet air temperature. This is because of the increase in the system thermal load. On the other hand, a maximum occurs in the specific flow rate of the cooling water upon the increase in the water inlet temperature. This is because of the continuous decrease in the air and water flow rates in the system. Therefore, the increase in the water temperature together with the decrease in the flow rates would generate a maximum the thermal load of the condenser, which in turn would cause a maximum in the specific flow rate of the cooling water.

As shown in Fig. 11, increase in the air temperature increases the driving force for heat transfer and as a result reduces the heat transfer area. The maximum occurring in the specific heat transfer area shown in Fig. 11 is caused by the same effects discussed for Fig. 10.

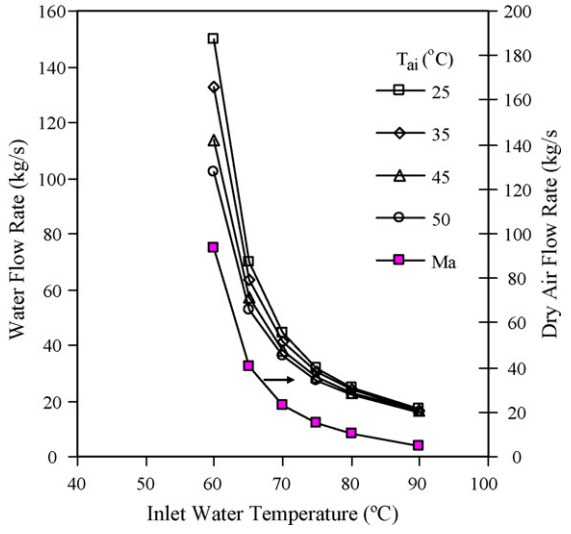

Fig. 8. Variation in the flow rates of dry air and water as a function of the intake air temperature and inlet water temperature.

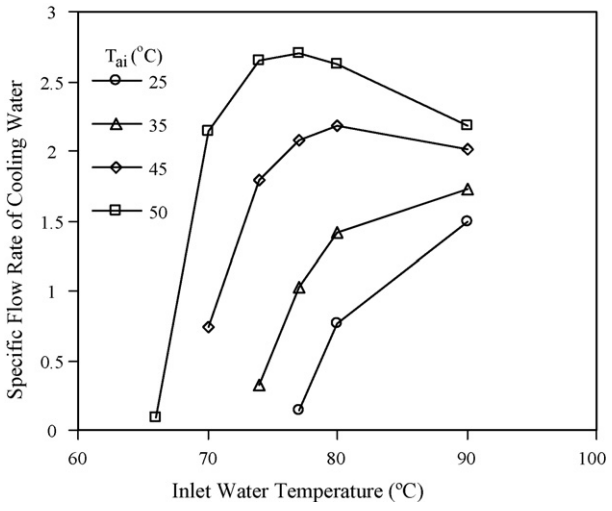

Fig. 10. Variation in the specific flow rate of cooling water as a function of the inlet temperatures of the air and water streams.

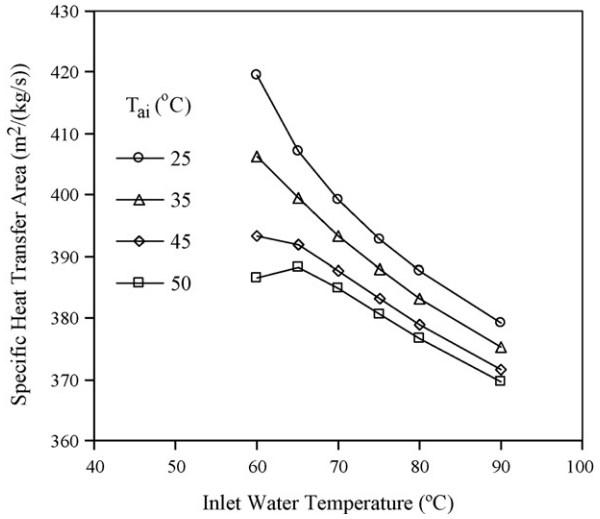

Fig. 11. Variation in the specific heat transfer area of the condenser as a function of the inlet temperatures of the air and water streams.

6. Conclusions

Design and analysis of the HDH system is presented through experimental measurements and mathematical modeling. A correlation is developed for the heat transfer coefficient for the humid air side in a double pipe condenser. The measurements and correlation predictions show that the heat transfer coefficient for humid air with water vapor condensation is almost 10 times that for dry air. Irrespective of that, the heat transfer coefficient is still small and it requires use of finned tube heat exchanger. This is because finned tube exchangers provide a heat transfer area ten times larger than a shell tube configuration. Characteristics of the HDH system are quite similar to a single-stage thermal desalination systems with vapor compression, where the performance ratio is greater than one, the specific heat transfer area for the condenser is around 300 $m^2/(kg\,s)$, and the specific flow rate of cooling water is around 3. It should be noted that such characteristics are obtained for desirable thermal parameters, where the temperatures of the outlet streams are close to the temperature of the intake streams. Further system optimization is highly recommended to determine the best design and operating conditions, which gives the lowest unit product cost. Proper system optimization would require measurements of the overall heat transfer and development of a correlation for the heat transfer coefficient for the air side in a finned tube condenser, which is the industry standard for air heat exchangers.

Appendix A

The water specific heat at constant pressure is given by

$$\mathrm{Cp} = (4206.8 - 1.1262\,T + 1.2026\times10^{-2}\,T^2 + 6.8777\times10^{-7}\,T^3)\times10^{-3} \quad (21)$$

where T is the temperature in °C and Cp is in kJ/(kg K) [13].

The density correlation for seawater is given by

$$\rho = 10^3(A_1F_1 + A_2F_2 + A_3F_3 + A_4F_4) \quad (22)$$

where $B = ((2)(X)/1000 - 150)/150$; $G_1 = 0.5$; $G_2 = B$; $G_3 = 2B^2 - 1$; $A_1 = 4.032219G_1 + 0.115313G_2 + 3.26\times10^{-4}G_3$; $A_2 = -0.108199G_1 + 1.571\times10^{-3}G_2 - 4.23\times10^{-4}G_3$; $A_3 = -0.012247G_1 + 1.74\times10^{-3}G_2 - 9\times10^{-6}G_3$; $A_4 = 6.92\times10^{-4}G_1 - 8.7\times10^{-5}G_2 - 5.3\times10^{-5}G_3$; $A = ((2)(T) - 200)/160$; $F_1 = 0.5$, $F_2 = A$, $F_3 = 2A^2 - 1$, $F_4 = 4A^3 - 3A$.

In the above equations ρ is the seawater density in kg/m^3, X is the seawater salinity in ppm, and T is the seawater temperature in °C. This correlation is valid over the following ranges: $0 \le X \le 160{,}000$ ppm and $10 \le T \le 180$ °C [13].

The correlation for the dynamic viscosity of seawater is given by

$$\mu = \mu_W\mu_R \times 10^{-3} \quad (23)$$

with

$$\ln(\mu_W) = -3.79418 + 604.129/(139.18 + T)$$

$$\mu_R = 1 + As + Bs^2$$

$$A = 1.474\times10^{-3} + 1.5\times10^{-5}\,T - 3.927\times10^{-8}\,T^2$$

$$B = 1.0734\times10^{-5} - 8.5\times10^{-8}\,T + 2.23\times10^{-10}\,T^2$$

where μ in kg/(m s), T in °C, and s in g/kg. The above correlation is valid over the following ranges $0 \le s \le 130$ g/kg and $10 \le T \le 180$ °C [13].

The water thermal conductivity is given by

$$\log_{10}(k) = \log_{10}(240 + A\ s) + 0.434\left(2.3 - \frac{343.5 + B\ s}{T + 273.15}\right)\left(1 - \frac{T + 273.15}{647.3 + C\ s}\right)^{1/3} \quad (24)$$

where k is the thermal conductivity in W/(m °C), s is the salinity in g/kg, T is the temperature in °C. The constants A, B, and C are equal to 2×10^{-4}, 3.7×10^{-2}, and 3×10^{-2}, respectively. The above correlation is valid over the following ranges, $0 \le s \le 160$ g/kg and $20 \le T \le 180$ °C [12].

The correlation for latent heat of water evaporation is given by the following correlation, which valid over a temperature range of 5–200 °C.

$$\lambda = 2501.897149 - 2.407064037\,T + 1.192217\times10^{-3}\,T^2 - 1.5863\times10^{-5}\,T^3 \quad (25)$$

In the above equation, T is the saturation temperature in °C and λ is the latent heat in kJ/kg.

The specific heat at constant pressure of air is given by the following correlation, which is valid over a temperature range of $250 < T < 1050$ K [14].

$$\mathrm{Cp} = 1.03409 - 2.84887\times10^{-4}\,T + 7.816818\times10^{-7}\,T^2 - 4.970786\times10^{-10}\,T^3 + 1.077024\times10^{-13}\,T^4 \quad (26)$$

In the above equation T is in K and Cp is in kJ/(kg K).

The air density is calculated from ideal gas law, which is valid for low pressures

$$\rho = \frac{p\bar{M}}{RT} \quad (27)$$

In the above equation ρ is the density in kg/m^3, p is the pressure in Pa, $\bar{M}$ is the molecular weight (for air, $\bar{M} = 28.966$), and R is the universal gas constant and is equal to 8315 Pa m^3/(kmol K).

The thermal conductivity of air is given by the following correlation, which is valid over a temperature range of $250 < T < 1050$ K [14].

$$k = 1\times10^{-3}(-2.276501\times10^{-3} + 1.2598485\times10^{-4}\,T - 1.4815235\times10^{-7}\,T^2 + 1.73550646\times10^{-10}\,T^3 - 1.066657\times10^{-13}\,T^4 + 2.47663035\times10^{-17}\,T^5) \quad (28)$$

In the above equation T is in K and k is in kW/(m K).

The dynamic viscosity of air is given by the following correlation, which is valid over a temperature range of $250 < T < 600$ K [14].

$$\mu = 1 \times 10^{-6}(-0.98601 + 9.080125 \times 10^{-2}\, T - 1.17635575 \times 10^{-4}\, T^2 + 1.2349703 \times 10^{-7}\, T^3 - 5.7971299 \times 10^{-11}\, T^4) \quad (29)$$

In the above equation T is in K and μ is in kg/(m s).

References

[1] The 19th IDA Worldwide Desalting Plant Inventory, International Desalination Association, Topsfield, MA, USA, 2006.
[2] M.F.A. Goosen, S.S. Sablani, W.H. Shayya, C. Paton, H. Al-Hinai, Thermodynamic and economic consideration in solar desalination, Desalination 129 (2000) 63–89.
[3] H. Muller-Holst, M. Engelhardt, W. Scholkopf, Small-scale thermal seawater desalination simulation and optimization of system design, Desalination 122 (1999) 255–262.
[4] M. Farid, A. Al-Hajaj, Solar desalination with a humidification–dehumidification cycle, Desalination 106 (1999) 427–429.
[5] S. Al-Hallaj, M.M. Farid, A. Tamimi, Solar desalination with a humidification–dehumidification cycle performance of the unit, Desalination 120 (1998) 273–280.
[6] N.K. Nawayseh, M.M. Farid, A. Omar, S.M. Al-Hallaj, A. Tamimi, A simulation study to improve the performance of a solar humidification–dehumidification desalination unit constructed in Jordan, Desalination 109 (1997) 277–284.
[7] N.K. Nawayseh, M.M. Farid, S. Al-Hallaj, A. Al-Timimi, Solar desalination based on humidification process. I. Evaluating the heat and mass transfer coefficients, Energy Convers. Manag. 40 (1999) 1423–1439.
[8] N.K. Nawayseh, M.M. Farid, A. Omar, A. Sabirin, Solar desalination based on humidification process. II. Computer simulation, Energy Convers. Manag. 40 (1999) 1441–1461.
[9] G. Al-Enezi, H.M. Ettouney, N. Fawzi, Low temperature humidification dehumidification desalination process, Energy Convers. Manag. 47 (2006) 470–484.
[10] H. Ettouney, Design and analysis of humidification dehumidification desalination process, Desalination 183 (3) (2005) 41–352.
[11] G.F. Hewitt, Heat Exchanger Design Handbook, Begelle House Inc., New York, 1998.
[12] A.S. Fouset, L.A. Wenzel, C.W. Clump, L. Maus, L.B. Andersen, Principles of Unit Operations, Wiley, New York, USA, 1980.
[13] H.T. El-Dessouky, H.M. Ettouney, Fundamentals of Salt Water Desalination, Elsevier, New York, 2002.
[14] J.P. Rohsenow, J.P. Hartnett, Y.I. Chao, Handbook of Heat Transfer, McGraw-Hill, New York, 1998.